Published in final edited form as:
*J Org Chem*. 2009 February 6; 74(3): 1070–1081. doi:10.1021/jo802037v.

# Functionalized 2′-Amino-α-L-LNA - Directed Positioning of Intercalators for DNA Targeting

**T. Santhosh Kumar**[†], **Andreas S. Madsen**[†], **Michael E. Østergaard**[‡], **Sujay P. Sau**[‡], **Jesper Wengel**[†], and **Patrick J. Hrdlicka**[‡]

[†]Nucleic Acid Center, University of Southern Denmark, DK-5230 Odense M, Denmark

[||]Department of Physics and Chemistry, University of Southern Denmark, DK-5230 Odense M, Denmark

[‡]Department of Chemistry, University of Idaho, Moscow, ID 83843-2343, USA.

## Abstract

Chemically modified oligonucleotides are increasingly applied in nucleic acid based therapeutics and diagnostics. LNA (Locked Nucleic Acid) and its diastereomer α-L-LNA are two promising examples hereof that exhibit increased thermal and enzymatic stability. Herein, the synthesis, biophysical characterization and molecular modeling of N2′-functionalized 2′-amino-α-L-LNA is described. Chemoselective N2′-functionalization of protected amino alcohol **1** followed by phosphitylation afforded a structurally varied set of target phosphoramidites, which were incorporated into oligodeoxyribonucleotides. Incorporation of pyrene-functionalized building blocks such as 2′-*N*-(pyren-1-yl)carbonyl-2′-amino-α-L-LNA (monomer **X**) led to extraordinary increases in thermal affinity of up to +19.5 °C per modification against DNA targets in particular. In contrast, incorporation of building blocks with small non-aromatic N2′-functionalities such as 2′-*N*-acetyl-2′-amino-α-L-LNA (monomer **V**) had detrimental effects on thermal affinity toward DNA/RNA complements with decreases of as much as −16.5 °C per modification. Extensive thermal DNA selectivity, favorable entropic contributions upon duplex formation, hybridization-induced bathochromic shifts of pyrene absorption maxima and increases of circular dichroism signals, and molecular modeling studies suggest that pyrene functionalized 2′-amino-α-L-LNA monomers **W**-**Y** having short linkers between the bicyclic skeleton and the pyrene moiety, allow high-affinity hybridization with DNA complements and precise positioning of intercalators in nucleic acid duplexes. This rigorous positional control has been utilized for the development probes for emerging therapeutic and diagnostic applications focusing on DNA-targeting.

## Introduction

Oligonucleotides are widely used for modulation of gene expression (e.g., antigene/antisense/siRNA),[1] for detection of nucleic acid targets,[2] and as building blocks of novel self-assembling

hrdlicka@uidaho.edu .

**Supporting Information Available:** General experimental section; experimental section for synthesis of nucleosides **2** and **3** (**V**/**W**/**Y**/**Z**-series); copies of $^{1}$H NMR, $^{13}$C NMR, $^{31}$P NMR, $^{1}$H-$^{1}$H COSY and/or $^{1}$H-$^{13}$C HETCOR spectra for all novel nucleosides; protocols for RP-HPLC and ion exchange HPLC purification of ONs; MALDI-MS of synthesized ONs (Table S3); representative thermal denaturation curves (Fig. S1); $T_m$-values of N2′-functionalized 2′-amino-α-L-LNA at various ionic strengths (Table S4); discussion of sequence dependent variation of $T_m$-values; DNA-selectivity of N2′-functionalized 2′-amino-α-L-LNA (Table S5); thermodynamic data for **B1**-**B5** (Table S6); protocol for acquisition and listing of additional CD-spectra (Fig. S2); protocol for molecular modeling studies; additional molecular modeling structures (Figs. S3-S9 and S11-S12), illustration of intercalation (Fig. S10); pseudorotational phase angle *P* and glycosidic torsion angle $\chi$ observed in simulated duplexes (Tables S7 and S8). This material is available free of charge via the Internet at http://pubs.acs.org.

biomaterials.[3] Chemical modification of oligonucleotides is often required to provide adequate protection from enzymatic degradation, to facilitate strong binding to complementary nucleic acid targets and to add functionality to oligonucleotides. Incorporation of conformationally restricted nucleotide monomers into oligonucleotides is a popular approach toward this end.[4,5] Locked nucleic acid (LNA, *β*-D-*ribo* configuration, Fig. 1) is a very promising member of this class of compounds. LNA[6-8] exhibits increases in thermal affinity toward DNA/RNA complements of up to +10 °C per modification along with markedly improved enzymatic stability relative to unmodified oligodeoxyribonucleotides (ONs).[9,10] These properties render LNA with high therapeutic and diagnostic potential,[11-14] which is underlined by ongoing Phase I/II clinical evaluations of LNA drug candidates against a variety of diseases. One of the diastereoisomers of LNA, i.e., α-L-LNA[6,15] (*α*-L-*ribo* configuration, monomer **O**, Fig. 1) shares the beneficial properties of LNA and has been used as antisense ONs,[16-18] triplex forming ONs,[19] modified DNAzymes,[20] and transcription factor decoy ONs.[21]

We have previously taken advantage of the known high-affinity hybridizations of 2′-amino-LNA[6,22] (Fig. 1) to develop a series of N2′-functionalized 2′-amino-LNA, which precisely position functional entities in the minor groove of nucleic acid duplexes without compromising duplex stability.[23] This has resulted in the development of tools for applications within therapeutics, diagnostics and material science including: a) probes yielding brightly fluorescent duplexes upon hybridization to complementary DNA/RNA with quantum yields approaching unity,[23d,23k] b) probes for single nucleotide polymorphism (SNP) detection,[23b, 23h] c) nucleic acid architectures auto signaling their self-assembly,[23b,23h] and d) artificial dinuclear ribonucleases.[23j]

Stimulated by these findings, we recently developed a synthetic route to 2′-amino-α-L-LNA (α-L-*ribo* configuration, monomer **Q**, Fig. 1),[6,24] and N2′-functionalized analogs thereof (Fig. 1). Appended functional entities were anticipated to be positioned in the *major groove* of nucleic acid duplexes.[24a] However, initial studies with N2′-pyrene-functionalized 2′-amino-α-L-LNA suggest that the conjugated functional entity is directed toward the duplex core instead.[25,26] This has already resulted in the development of promising tools for DNA-targeting,[25a] detection of single nucleotide polymorphisms[25b] and nucleic acid structural engineering.[25d]

Herein, full experimental details on the synthesis of a structurally varied set of N2′-functionalized 2′-amino-α-L-LNA phosphoramidites and their incorporation into ONs are presented (Fig. 1). Results from biophysical and computational studies are discussed together with the suggested binding mode of the appended functional entities.

## Results and Discussion

### Synthesis of N2′-functionalized 2′-amino-α-L-LNA

Known O5′-tritylated bicyclic nucleoside **1**[24b], which is obtained from commercially available diacetone-α-D-glucose in 5% overall yield over seventeen steps involving eight chromatographic purification steps, was used as a suitable starting material for the synthesis of N2′-functionalized 2′-amino-α-L-LNA phosphoramidites **3Q-3Z** (Scheme 1). The targets were selected to probe the available structural space in nucleic acid duplexes and fall into two groups based on the nature of the N2’-moiety, i.e., monomers with small non-aromatic units (monomers **Q, S**, and **V**) or with aromatic units (monomers **W**-**Z**). Sodium triacetoxyborohydride mediated reductive amination[27] of secondary amine **1** with acetaldehyde or 1-pyrenecarbaldehyde furnished tertiary amines **2S** and **2W**[25a] in 48% and 67% yield, respectively. Chemoselective *N*-acylation of amino alcohol **1** was achieved using two different strategies. Treatment of nucleoside **1** with slight excess of acetic anhydride followed by selective O3′-deacylation using dilute methanolic ammonia furnished nucleoside

**2V** in excellent 88% yield over two steps. EDC-mediated coupling of amino alcohol **1** with 1-pyrenylcarboxylic acid, 1-pyrenylacetic acid or 4-(1-pyrenyl)butyric acid afforded nucleosides **2X, 2Y**[25b,25d] and **2Z** in 62%, 86% and 63% yield, respectively. A HATU-mediated (*O*-(7-azabenzotriazole-1-yl)-*N*,*N*,*N*′,*N*′-tetramethyluronium hexafluorophosphate) coupling procedure successfully improved the yield of **2X** to 90%. Disappearance of $^1$H NMR signals of the exchangeable 3′-OH protons upon $D_2O$ addition ascertained the N2′-functionalized constitution of nucleosides **2S-2Z**, which subsequently were converted to the corresponding phosphoramidites **3S-3Z** using 2-cyanoethyl *N*,*N*′-(diisopropyl)-phosphoramidochloridite and Hünig's base. While amidites **3S-3Y** were obtained in good to excellent yields (60-90 %), **3Z** was only obtained in 36% yield. The yield of **3X** was improved using bis-(*N*,*N*-diisopropylamino)-2-cyanoethoxyphosphine in dichloromethane with diisopropylammonium tetrazolide[28] as activator (71%). Synthesis of ONs was performed in 0.2 μmol scale using an automated DNA synthesizer. The corresponding phosphoramidites for incorporation of α-L-LNA thymine monomer **O** (obtained from commercial sources) and 2′-amino-α-L-LNA thymine monomer **Q** (synthesized by a previously described protocol)[24b] were incorporated into our preferred model system, i.e., a set of mixed sequence 9-mer ONs, as previously described.[15b,24b] Standard procedures were applied for incorporation of N2′-functionalized 2′-amino-α-L-LNA thymine monomers **S-Z** (Fig. 1) except for extended coupling times: **3S** (10 min), **3V** (10 min), **3W**[25a] (30 min), **3Y**[25b] (30 min), **3X** (30 min) and **3Z** (15 min)) using 1*H*-tetrazole as catalyst resulting in stepwise coupling yields of ~99% for monomers **S, V, X, Y, Z** and ~95% for monomer **W** (Fig. 1 for structures). Following standard workup and purification, the composition and purity (>80%) of all modified ONs was verified by MALDI-MS (Table S3)[29] and ion-exchange HPLC, respectively. Please **NOTE** that the unmodified reference DNA and RNA strands are denoted **D1/D2** and **R1/R2**, respectively, while ONs containing a single incorporation of a modified nucleotide in the 5′-G**B**G ATA TGC context are named **O1, Q1, S1** etc. Similar conventions were used for ONs in **B2-B7** series (Tables 1 and 2). In addition, the following descriptive nomenclature is used: α-L-amino-LNA (**Q**-series), Et α-L-amino-LNA (**S**-series), Ac-α-L-amino-LNA (**V**-series), PyMe-α-L-amino-LNA (**W**-series), PyCO-α-L-amino-LNA (**X**-series), PyAc-α-L-amino-LNA (**Y**-series) and PyBu-α-L-amino-LNA (**Z**-series).

## Thermal denaturation studies – experimental setup

The effect upon incorporation of one to three **O-Z** monomers (Fig. 1) into mixed sequence 9-mer ONs on thermal affinity toward DNA and RNA targets (Tables 1 and 2, respectively) was evaluated by UV thermal denaturation experiments using medium salt buffer ([$Na^+$] = 110 mM), and compared to unmodified DNA. The UV thermal denaturation curves of all modified duplexes exhibited sigmoidal monophasic transitions with hyperchromicities (9-15%) which are comparable to the corresponding unmodified DNA:DNA or DNA:RNA duplexes (Fig. S1).[29] All changes in thermal denaturation temperatures ($T_m$) of modified nucleic acid duplexes are discussed relative to $T_m$ values of unmodified reference duplexes unless otherwise mentioned. In addition, the Watson-Crick specificity of ONs with a single central incorporation of monomer **O-Z** (**B2**-series) was evaluated by determining $T_m$ values of the duplexes with DNA/RNA strands with central mismatches (Table 3).

## Thermal denaturation studies – α-L-LNA and 2′-amino-α-L-LNA – the reference ONs

α-L-LNA **O1-O5** exhibit substantially increased thermal affinity toward DNA ($\Delta T_m$ up to +8.0 °C, Table 1) and RNA complements ($\Delta T_m$ = up to +10.0 °C, Table 2). The corresponding 2′-amino-α-L-LNA **Q1-Q5** display notably smaller increases in thermal affinity ($\Delta T_m$ up to +2.5 °C with DNA, Table 1; $\Delta T_m$ up to +4.5 °C with RNA, Table 2). Similar $\Delta T_m$-values for duplexes between α-L-amino-LNA **Q4** and DNA/RNA complements determined at different ionic strengths were observed (Table S4),[29] suggesting that the 2-oxo-5-azabicyclo[2.2.1] heptane skeleton of monomer **Q** is not protonated at physiological pH. The increased binding

affinity of α-L-LNA and 2′-amino-α-L-LNA was accompanied by improved discrimination of singly mismatched DNA and RNA targets relative to unmodified DNA **D1** (e.g., $\Delta T_m$ values for α-L-amino-LNA **Q2** and **D1** against DNA mismatches, Table 3).

### Thermal denaturation studies – N2′-pyrene-functionalized 2′-amino-α-L-NA

Incorporation of a single PyMe/PyCO/PyAc-α-L-amino-LNA monomer **W, X** or **Y**, respectively, into ONs resulted in *extraordinary increases in thermal affinity* toward DNA complements ($\Delta T_m$ from +6.5 °C to +19.5 °C, Table 1). Moderate increases were observed upon incorporation of PyBu-α-L-amino-LNA monomer **Z** ($\Delta T_m$ up to +6.5 °C, Table 1). The observed trends in thermal affinity of singly modified strands toward DNA targets (**X** > **Y** > **W** >> **Z**) suggest that: a) alkanoyl linkers are thermally preferred over alkyl linkers of the same length (**X** > **W**), and b) shorter linkers are thermally preferred (**X** > **Y** >> **Z**). For a discussion on the sequence dependent variations of $T_m$-values observed for these ONs the reader is directed to the supporting information.[29] Interestingly, additive increases in thermal affinity toward DNA targets are observed upon multiple incorporations of PyAc-α-L-amino-LNA **Y** monomers (e.g., compare $T_m$/mod values of **Y6:D1, Y4:D1** and **Y5:D1**, Table 1), while subadditive increases are observed for the corresponding α-L-LNA **O6**, 2'-amino-α-L-LNA **Q6** or PyMe-α-L-amino-LNA **X6**. Thus, PyAc-α-L-amino-LNA monomer **Y** lends itself as the building block of choice for applications necessitating densely functionalized ONs with maximal thermal affinity toward DNA targets.

PyCO/PyAc-α-L-amino-LNA (**X1-X6** and **Y1-Y7**, respectively) exhibit prominent and additive increases in thermal affinity toward RNA complements ($\Delta T_m$ from +4.5 °C to +12.0 °C, Table 2). In contrast, minor destabilizations to moderate increases were observed for PyMe/PyBu-α-L-amino-LNA **W1-W5** and **Z1-Z5**, respectively, with the exception of **Z4** which exhibited a very pronounced decrease in thermal affinity toward its RNA target (Table 2).

Accordingly, N2′-pyrene-functionalized 2′-amino-α-L-LNA exhibit a marked DNA selectivity, i.e., a positive $\Delta\Delta T_m$/mod (DNA-RNA) = $\Delta T_m$/mod (DNA) − $\Delta T_m$/mod (RNA). This is particularly noteworthy as the parent α-L-LNA and 2′-amino-α-L-LNA exhibit moderate RNA-selectivity ($\Delta\Delta T_m$/mod (DNA-RNA) = −3.5 to −1.7 °C, Tables 1 and 2 or, more conveniently, Table S5[29]). PyMe/PyCO-α-L-amino-LNA exhibit the most pronounced DNA selectivity ($\Delta\Delta T_m$/mod (DNA-RNA) = +6.0 to +9.0 °C, Table S5), suggesting that short linkers between the pyrene and nucleoside moieties facilitate DNA-selectivity. While PyMe/PyCO-α-L-amino-LNA exhibit a similar degree of DNA selectivity as acyclic intercalating nucleic acids (INAs),[30] 2′-*O*-pyrenylmethyl uridines[31] or pyrene-functionalized 4′-*C*-piperazinomethyl thymidines,[32] they generally form stronger duplexes with DNA targets, which renders them as highly interesting probes for DNA-targeting applications.[25a]

Centrally modified PyMe-α-L-amino-LNA **W2** exhibit less efficient discrimination of mismatched DNA/RNA targets than the corresponding reference strand **D1** (Table 3). Interestingly, a change in linker chemistry from methylene to carbonyl (**W→X**) results in higher affinity toward DNA/RNA complements as well as significantly improved mismatch discrimination (Table 3). With the exception of T:T/U mismatches, PyCO-α-L-amino-LNA **X2** displays mismatch discrimination comparable to reference strand **D1**. Increases in linker length result in progressively improved discrimination of DNA/RNA mismatches (compare $\Delta T_m$ data for **X2, Y2** and **Z2**, Table 3). Accordingly, PyBu-α-L-amino-LNA **Z2** exhibits superior discrimination of RNA mismatches in general, and of the challenging T:rG mismatch in particular ($\Delta T_m$ = −16.0 °C, data for **Z2**, Table 3), relative to the already highly discriminative α-L-LNA **O2**.

### Thermal denaturation studies – N2′-ethyl/acetyl-modified 2′-amino-α-L-LNA

Et-α-L-amino-LNAs **S1**-**S7** exhibit greatly decreased thermal affinities toward DNA/RNA targets in general and complementary DNA in particular ($\Delta T_m$/mod down to −12.0 °C, Table 1). These effects are even more pronounced with Ac-α-L-amino-LNA **V1**-**V7** which exhibit decreases in $T_m$ values down to −16.5 °C per modification (Table 1). Accordingly, no duplex transitions could be observed for ONs with two or three incorporations of **S** or **V** monomers and their DNA/RNA targets. Interestingly, the large decreases in thermal affinity toward DNA/RNA complements of Et/Ac-α-L-amino-LNA, generally did not compromise Watson-Crick specificity (see data for **S2** and **V2**, Table 3), which suggests that base-pairing is preserved.

It is noteworthy that an exchange of a centrally positioned PyCO-α-L-amino-LNA monomer **X** with a corresponding Ac-α-L-amino-LNA monomer **V** (i.e., a formal change of pyrene to methyl), was accompanied by a decrease in thermal affinity toward complementary DNA of 31.0 °C (compare $T_m$ values of **X2:D2** and **V2:D2**, Table 1). This suggests very different binding mode for ONs modified with monomers **S/V** and **W/Y**, respectively, which was underlined upon additional biophysical characterization (vide infra).

### Additional biophysical characterization of N2′-functionalized 2′-amino-α-L-LNA – experimental setup

To obtain additional insight into the highly divergent thermal affinities of N2′-functionalized 2′-amino-α-L-LNA the following biophysical studies were performed: a) determination of thermodynamic parameters for duplex formation, b) CD-spectra, c) UV-vis spectra (shifts of pyrene absorption maxima), and d) molecular modeling studies.

Thermodynamic parameters for duplex formation were determined by melting curve analysis assuming bimolecular reactions and two-state equilibrium hypothesis. Quality of the baseline permitting, thermodynamic parameters for two melting curves per investigated duplex were determined and an average value is listed. In full agreement with expectations, formation of all studied duplexes was favorable ($\Delta G^{298} < 0$ kJ/mol), with favorable enthalpic ($\Delta H < 0$ kJ/mol) and unfavorable entropic contributions ($T^{298}\Delta S < 0$ kJ/mol). The thermodynamic data rely on assumptions of two-state melting behavior and a heat capacity change $\Delta C_p = 0$ upon hybridization, which may not necessarily be fulfilled. However, apart from few exceptions (see footnote *a* in Table 4), the observed enthalpic/entropic contributions for hybridization of N2′-functionalized 2′-amino-α-L-LNA to DNA/RNA targets clearly followed monomer and sequence specific trends, which validates the utilized approach (data shown for the representative **B2**-series Tables 4 and 5; for data and full discussion of **B1**-**B5** series see Table S6[29]).

Duplexes between N2′-functionalized 2′-amino-α-L-LNA and DNA/RNA complements were studied by force field simulations. For this, DNA duplexes were built in silico and modified with an N2′-functionalized 2′-amino-α-L-LNA monomer. A starting B-type helix geometry was chosen as duplexes between α-L-LNA and DNA complements adopt helix geometries that are globally unperturbed relative to unmodified DNA:DNA duplexes.[33] ONs with centrally positioned modifications (**B2**-series) were selected for the simulations to minimize the influence of fraying on the helix geometry near the modified nucleotides. The position of N2′-functionalities was explored using a truncated Monte Carlo search,[29] and the partially constrained duplexes were subjected to stochastic dynamics simulations using the all-atom AMBER force field[34] and GB/SA solvation model[35] as implemented in the MacroModel V9.1 suite of programs.[36]

### Integrated structural discussion - α-L-LNA and 2′-amino-α-L-LNA – the reference ONs

The markedly increased thermal affinity of α-L-LNA **O1-O5** toward complementary DNA/RNA relative to unmodified ONs results from a more *favorable enthalpic term* that largely is counterbalanced by an *unfavorable entropic term*, i.e., $\Delta\Delta G_{298}$ (**O2**$_{\mathbf{DNA}}$) = $\Delta G_{298}$(**O2:D2**) − $\Delta G_{298}$(**D1:D2**) = −5 kJ/mol; ΔΔH (**O2**$_{\mathbf{DNA}}$) = ΔH(**O2:D2**) − ΔH(**D1:D2**) = −27 kJ/mol; Δ($T^{298}$ΔS) (**O2**$_{DNA}$) = $T^{298}$ ΔS (**O2:D2**) − $T^{298}$ΔS (**D1:D2**) = −22 kJ/mol (Table 4). This suggests that high thermal affinity of the conformationally restricted α-L-LNA **O1-O5** toward DNA/RNA complements is a result of a more favorable stacking/hydrogen bonding geometry and/or duplex solvation rather than preorganization of the single stranded probe.

Similarly, the hybridization of 2′-amino-α-L-LNA **Q1-Q5** to complementary RNA is also driven by favorable enthalpy that is partially counterbalanced by unfavorable entropy, although the individual contributions are less pronounced than for α-L-LNA **O1-O5** (e.g., ΔΔH = −86 kJ/mol and −27 kJ/mol for **O2**$_{\mathbf{RNA}}$ and **Q2**$_{\mathbf{RNA}}$, respectively, Table 4). The energetics for hybridization of **Q1-Q5** to DNA complements are sequence dependent and could not be fitted to a clear pattern, Tables 4 and S6[29]).

The applied molecular modeling protocol successfully reproduced expected global and local features of α-L-LNA duplex **O2:D2** (Fig. S4) providing credibility to the applied computational protocol. These features of **O2:D2** include a standard B-type global duplex geometry similar to **D1:D2** (Fig. S3) and very characteristic local perturbations in the backbone needed to accommodate the inverted configurations at the C2′-, C3′- and C4′-positions of α-L-LNA monomer **O**.[29,33] Interestingly, the global helix structures of **O2:D2** and **Q2:D2** (Fig. S5)[29] are virtually identical, which is validated by very similar circular dichroism spectra of **Q7:D2** and **O7:D2** (Fig. S2). Thus, different solvation patterns rather than substantially altered helical geometries likely account for the diverging energetics observed for these closely related ONs upon hybridization with DNA/RNA complements.

### Integrated structural discussion - N2′-ethyl/acetyl-modified 2′-amino-α-L-LNA

The dramatically destabilized duplexes between Et/Ac-α-L-amino-LNA and DNA/RNA targets ($\Delta\Delta G^{298}$ up to +12 kJ/mol) result from unfavorable entropic components that are only partially counterbalanced by favorable enthalpic components (e.g., Δ($T^{298}$ΔS) (**S2**$_{\mathbf{RNA}}$) = −84 kJ/mol and ΔΔH (**S2**$_{\mathbf{RNA}}$) = −77 kJ/mol, Table 4).

Intriguingly, very similar CD spectra are observed for **S2:D2, V2:D2** and the reference duplex **D1:D2** suggesting that incorporation of **S** and **V** monomers renders these duplexes globally unperturbed while dramatically lowering stability (Fig 2). In accordance with this, the lowest energy structures of Et-α-L-amino-LNA duplex **S2:D2** (Figs. 3 and S6) and Ac-α-L-amino-LNA duplex **V2:D2** (Figs. 3 and S7) globally resembled each other and α-L-amino-LNA duplex **Q2:D2** (Fig. S5).[29] In **S2:D2** the ethyl group of **S**$_{\mathbf{5}}$ protrudes from the major groove valley to become involved in a steric clash with H5′ of **A**$_{\mathbf{6}}$ (for numbering scheme see Fig. 4). We speculate that unfavorable desolvation of the apolar ethyl moiety (whereby fewer water molecules are released) and interference with structural water along the sugar-phosphate backbone,[37,38] in a similar manner as proposed for monomer **Q**,[29] accounts for the unfavorable entropy observed upon hybridization of Et-α-L-amino-LNA **S2** with DNA/RNA targets (Table 4). In a related manner, one part of the N2′-acetyl moiety of monomer **V** (i.e., either the -CO- or -$CH_3$) in **V2:D2** is directed toward the major groove where it can interfere with structural water while the other part simultaneously protrudes into the duplex core to disrupt π-π stacking (Figs. 3 and S7).[29]

To sum up, biophysical characterization and computer simulations jointly suggest that N2′-functionalization of 2′-amino-α-L-LNA, contrary to preliminary expectations,[24a] is not suitable

to position small non-aromatic moieties in the major groove of duplexes with DNA or RNA complements.

### Integrated structural discussion - N2′-pyrene-functionalized 2′-amino-α-L-LNA

The very pronounced stabilization of duplexes between PyMe-α-L-amino-LNA or PyAc-α-L-amino-LNA and complementary DNA (e.g. $\Delta\Delta G_{298}$ (**W2$_{DNA}$**) = −12 kJ/mol) *results from highly favorable entropy* (e.g. $\Delta\Delta(T^{298}\Delta S)$ (**W2$_{DNA}$**) = +32 kJ/mol, Table 5). Stabilization of duplexes between PyCO-α-L-amino-LNA and DNA targets (e.g. $\Delta\Delta G^{298}$ (**X2$_{DNA}$**) = −18 kJ/mol) is to a greater extent *driven by favorable enthalpic factors*. The moderate stabilization of duplexes between PyBu-α-L-amino-LNA and DNA complements (e.g. $\Delta\Delta G^{298}$ (**Z2$_{DNA}$**) = −5 kJ/mol), originates from favorable enthalpy contributions that mostly were counterbalanced by unfavorable entropy components ($\Delta\Delta H$ (**Z2$_{DNA}$**) = −9 kJ/mol, $\Delta(T^{298}\Delta S)$ (**Z2$_{DNA}$**) = −4 kJ/mol, Table 5).

The observed stabilization of duplexes between PyMe/PyCO/PyAc-α-L-amino-LNA with RNA complements results from favorable enthalpy ($\Delta\Delta H$ = −53 kJ/mol, −68 kJ/mol and −58 kJ/mol for **W2$_{RNA}$, X2$_{RNA}$** and **Y2$_{RNA}$**, respectively). However, comparison with 2′-amino-α-L-LNA reference strands instead of unmodified DNA suggests that *entropic contributions also aid duplex formation* with RNA targets (e.g. $\Delta(T^{298}\Delta S)$ = −17 kJ/mol, −28 kJ/mol, −17 kJ/mol and −51 kJ/mol for **W3$_{RNA}$, X3$_{RNA}$, Y3$_{RNA}$** and **Q3$_{RNA}$**, respectively, Table S6).[29]

Thus, energetics suggest that N2'-pyrene-functionalized 2'-amino-α-L-LNA exhibit binding modes that rely on preorganization unlike than 2'-amino-α-L-LNA modified with non-aromatic moieties.

The pronounced DNA-selectivity of PyMe/PyCO/PyAc-α-L-amino-LNA suggests intercalation of the pyrene moieties as a likely binding mode.[30-32,39] The CD spectra of PyAc-α-L-amino-LNA and duplexes with complementary DNA/RNA support this hypothesis as induced CD bands in the region of pyrene absorption (λ = 320-360 nm, Fig. 5), a feature indicative of intercalation,[40] are observed upon hybridization. In addition, marked bathochromic shifts of pyrene absorption maxima of ONs containing monomers **W**-**Y** upon hybridization with DNA/RNA targets ($\Delta\lambda_{max}$ = 1-5 nm and 0-6 nm, respectively, Table 6) along with hypochromic shifts (illustrated for **W2** and **Y2**, Fig. 6) suggest strong electronic interactions between the pyrene and nucleobase moieties in duplexes.[40-42] A change in linker chemistry from alkyl to alkanoyl (PyMe-α-L-amino-LNA **W** → PyCO-α-L-amino-LNA **X**) resulted in small but consistently larger hybridization-induced bathochromic shifts, while further extension of the alkanoyl linker (PyCO-α-L-amino-LNA **X** → PyAc-α-L-amino-LNA **Y** → PyBu-α-L-amino-LNA **Z**) progressively reversed this trend. The very subtle hybridization-induced bathochromic shifts of pyrene absorption maxima observed with PyBu-α-L-amino-LNA indicate a non intercalating binding mode of the pyrene moiety of monomer **Z** (Table 6).

In full agreement with biophysical data, the lowest energy structure of the duplex between PyMe-α-L-amino-LNA **W2** and complementary DNA **D2** suggests precise intercalation of the pyrene moiety (Fig. 7). It is imperative to stress that the utilized simulation protocol did not initiate from a structure where the pyrene moiety was intercalated, i.e., the pyrene moiety moved from an extrahelical to an intercalated position during the simulation. As expected[43] significant global unwinding, concomitant lengthening of the duplex and widening of the minor groove was observed upon intercalation. The pyrene moiety forms extensive π-π stacks with the nucleobase moieties of **W$_5$** and the 3′-flanking **A$_6$** and to a lesser extent with the nucleobase moieties of **T$_{13}$** and **A$_{14}$**. The pseudorotational phase angle P and glycosidic torsion angle $\chi$[44] of PyMe-α-L-amino-LNA monomer **W** change little relative to the 2′-amino-α-L-LNA monomer in **Q2:D2**. However, P and $\chi$ of the adjacent **A$_6$** moiety increase markedly in response

to intercalation (*P* from 97° to 127 °, and $\chi$ from −147 ° to −105 °, for **Q2:D2** and **W2:D2**, respectively, Tables S7 and S8),[29] to facilitate efficient π-π stacking between the pyrene and nucleobase moieties.

The lowest energy structures of duplexes between PyCO-α-L-amino-LNA **X2** or PyAc-α-L-amino-LNA **Y2** and complementary DNA **D2** (Figs. 8, S8 and S9),[29] exhibited similar key features as **W2:D2**, i.e., intercalation of the pyrene moiety and efficient π-π overlapping with flanking base pairs, similar sugar puckers and glycosidic torsion angles for $\mathbf{X_5/Y_5}$ and $\mathbf{A_6}$, and unwinding of the duplex and widening of the grooves.[29] Two minor structural differences observed with PyAc-α-L-amino-LNA duplex **Y2:D2** (Figs. 8 and S9) relative to **W2:D2** (Fig. 7) or **X2:D2** (Figs. 8 and S8) included increased stacking interactions with $\mathbf{T_{13}}$ and $\mathbf{A_{14}}$ and an altered orientation of the pyrene moiety, i.e., $H3_{py}$ and $H4_{py}$ of monomer **Y** face the major groove while facing the minor groove in **W2:D2** and **X2:D2** (Fig. S10).[29] Closer scrutiny of the molecular arrangement in PyMe/PyCO/PyAc-α-L-amino-LNA monomers **W-Y** reveals that the attachment points of the nucleobase and pyrene moieties (i.e., C1′ and N2′, respectively) are efficiently locked relative to each other (Fig. 9) as a consequence of the 2-oxo-5-azabicyclo [2.2.1]heptane skeleton. This, in concert with the short linker between the bicyclic skeleton and pyrene moiety and the strength of π-π stacking in aqueous environments, de facto directs the pyrene moiety of monomers **W-Y** into the duplex core to facilitate intercalation. This molecular arrangement leads to π-π stacking with the $\mathbf{T_5{:}A_{14}}$ and $\mathbf{A_6{:}T_{13}}$ base pairs and a reduction in buckle and propeller twist fluctuation in this nucleotide step (results not shown) to form a highly stablilized duplex segment. The observed thermodynamic data for PyMe/PyCO/PyAc-α-L-amino-LNA are in agreement with this preorganized binding mode of the pyrene as favorable entropic components were identified as important factors for duplex stabilization (Table 5). Desolvation upon intercalation of the highly apolar pyrene moiety is also likely to result in additional favorable entropic contributions upon duplex formation. Since the observed modeling structures of **W2:D2, X2:D2** and **Y2:D2** are very similar, it is likely that differential solvation of the single stranded probes or of their duplexes with DNA/RNA complements accounts for the observed differences in thermal affinity toward nucleic acid targets. For example, less pronounced desolvation of PyCO-α-L-amino-LNA **X2** relative to PyMe-α-L-amino-LNA **W2** upon hybridization to complementary DNA may account for less favorable entropy (fewer water molecules free upon hybridization) and more favorable enthalpy (formation of hydrogen bonds with surrounding water molecules).

The binding mode of the pyrene moiety of PyBu-α-L-amino-LNA was expected to be more ambiguous since: a) **Z1-Z5** exhibited lower increases in thermal affinity toward DNA complements in particular (Table 1), b) **Z2** displayed markedly improved mismatch discrimination relative to PyMe/PyCO/PyAc-α-L-amino-LNA (Table 3), and c) more subtle hybridization-induced bathochromic shifts of pyrene absorption maxima were observed (Table 6). In full agreement with these biophysical observations, molecular modeling suggested at least two different binding modes. An intercalated binding mode was observed that exhibited the hallmarks described above for **W2-Y2:D2** (Fig. S11). The model structure suggested that the long and relatively bulky butanoyl linker of PyBu-α-L-amino-LNA monomer **Z**: a) reduced π-π overlap between the pyrene and the nucleobase moieties of $\mathbf{Z_5}$ and $\mathbf{A_6}$ to a minimum, while increasing overlap with $\mathbf{T_{13}}$ and $\mathbf{A_{14}}$, b) was wedged into the duplex core in between $\mathbf{Z_5}$ and $\mathbf{A_6}$ to locally perturb the duplex and introduce a kink, and c) oriented the pyrene moiety with the $H3_{pyr}$ and $H4_{pyr}$ sides facing the major groove (Fig. S10).[29]

The second binding mode that is more in line with observations, the pyrene moiety is located at the floor of the major groove and is involved in non-specific contacts with the Hoogsteen faces of $\mathbf{A_6, C_{11}, A_{12}}$ and $\mathbf{T_{13}}$ (Figs. 8 and S12).[29] Minor groove binders conjugated to ONs are well known to increase the strength and specificity of hybridization.[45,46] By analogy, major groove binding of the pyrene moiety of monomer **Z** may explain the observed increased

mismatch discrimination of **Z2** (Table 3). Thus, biophysical characterization and computer simulations indicate that PyBu-α-L-LNA may stabilize duplexes with DNA/RNA complements by a wider variety of binding modes than PyMe/PyCO/PyAc-α-L-LNA exhibiting shorter linkers between the bicyclic skeleton and pyrene moiety.

## Conclusion

Herein we demonstrate that the 2-oxo-5-azabicyclo[2.2.1]heptane skeleton of 2'-amino-α-L-LNA, in concert with short linkers, directs intercalators appended to the N2'-position very effectively to the nucleic acid cores. Consequently, dramatic increases in thermal affinity toward DNA complements of up to +19.5 °C per modification are observed. Directed positioning of intercalators inside nucleic acid duplex cores has many potential interesting applications within nucleic acid based diagnostics, therapeutics and nanotechnology,[47] including detection of DNA/RNA complements and/or single nucleotide polymorphisms by fluorescence,[25b,30a,48-50] study of charge transfer processes,[51] formation of metal ion arrays within nucleic acid duplex cores,[52,53] or development of artificial nucleases.[54] Unlike previously reported building blocks, N2′-intercalator-functionalized 2′-amino-α-L-LNA effectively combines high-affinity hybridization with DNA complements and precise positioning of intercalators in nucleic acid duplexes. We propose N2'-intercalator-modified 2'-amino-α-L-LNA monomers as highly valuable monomers for established and emerging DNA-targeting applications.

## Experimental Section

### (1*S*,3*R*,4*S*,7*R*)-1-(4,4′-Dimethoxytrityloxymethyl)-5-ethyl-7-hydroxy-3-(thymin-1-yl)-2-oxa-5-azabicyclo[2.2.1]heptane 2S

Amino alcohol **1** (0.40 g, 0.70 mmol) was coevaporated with anhydrous 1,2-dichloroethane (2 × 8 mL) and dissolved in anhydrous 1,2-dichloroethane (8 mL). To this were added $NaBH(OAc)_3$ (230 mg, 1.09 mmol) and $CH_3CHO$ (44 μL, 0.78 mmol) and after stirring the reaction mixture at rt for 40 h, it was diluted with EtOAc (35 mL) and washed with sat. aq. $NaHCO_3$ (2 × 15 mL). The organic phase was evaporated to dryness and the resulting residue purified by silica gel column chromatography (0-5% *i*-PrOH in $CH_2Cl_2$, v/v) to afford nucleoside **2S** (200 mg, 48%). $R_f$ = 0.5 (10% MeOH in $CH_2Cl_2$, v/v); MALDI-HRMS *m/z* 622.2524 ($[M + Na]^+$, $C_{34}H_{37}N_3O_7Na^+$ Calcd 622.2522); $^1$H NMR (DMSO-$d_6$)[55] $\delta$ 11.26 (s, 1H, ex, NH), 7.49 (s, 1H, H-6), 7.21-7.44 (m, 9H, Ar), 6.87-6.92 (d, 4H, *J* = 8.8 Hz, Ar), 5.91 (d, 1H, *J* = 1.5 Hz, H-1′), 5.70 (d, 1H, ex, *J* = 3.5 Hz, 3′-OH), 4.31 (d, 1H, *J* = 3.5 Hz, H-3′), 3.74 (s, 6H, 2 × $CH_3O$), 3.19-3.30 (m, 4H, H-2′, 2 × H-5′, H-5″), 2.64-2.83 (m, 3H, $CH_2CH_3$, H-5″), 1.83 (s, 3H, $CH_3Ar$), 0.82 (t, 3H, *J* = 7.3 Hz, $CH_3$). $^{13}$C NMR (DMSO-$d_6$) $\delta$ 163.8, 158.0, 150.3, 144.8, 137.4, 135.4, 135.3, 129.7, 127.8, 127.6, 126.6, 113.1, 105.9, 90.0, 85.0, 74.4, 65.4, 60.8, 58.3, 54.9, 49.5, 14.8, 12.2; Anal. Calc. for $C_{34}H_{37}N_3O_7$: C, 68.10; H, 6.22; N, 7.01; Found: C, 67.96; H, 6.37; N, 6.54. Calcd with 1/8 *i*-PrOH: C, 68.00; H, 6.31; N, 6.92.

### (1*S*,3*R*,4*S*,7*R*)-1-(4,4′-Dimethoxytrityloxymethyl)-7-hydroxy-5-(pyren-1-yl)carbonyl-3-(thymin-1-yl)-2-oxa-5-azabicyclo[2.2.1]heptane 2X

1-Pyrenylcarboxylic acid (162 mg, 0.65 mmol), O-(7-Azabenzotriazole-1-yl)-*N*,*N*,*N*′,*N*′-tetramethyluronium hexafluorophosphate (HATU, 183 mg, 0.48 mmol) and *N*,*N*′-diisopropylethylamine (0.19 mL, 1.1 mmol) were dissolved in anhydrous DMF (4.2 mL) and the mixture was allowed to stir for 6 h at rt. To this was added a solution of nucleoside **1** (0.25 g, 0.44 mmol), which had been dried by coevaporation with anhydrous toulene (2 × 10 mL) ahead of time, dissolved in anhydrous DMF (4.2 mL). After stirring at rt for 12 h, the reaction mixture was diluted with $CH_2Cl_2$ (50 mL), washed with sat. aq. $NaHCO_3$ (10 mL) and $H_2O$ (4 × 10 mL). The aqueous phase was back extracted with $CH_2Cl_2$ (2 × 30 mL), and the combined

organic phase was evaporated to dryness, and resulting crude residue adsorbed on silica gel and purified by silica gel column chromatography (0-4% MeOH in $CH_2Cl_2$, v/v) to afford a rotameric mixture (~1:1.4 by $^1$H NMR) of nucleoside **2X** as a white solid material (0.32 g, 90%). $R_f$ = 0.2 (50% acetone in petroleum ether, v/v), MALDI-HRMS *m/z* 822.2786 ([M + Na]$^+$, $C_{49}H_{41}N_3O_8{\cdot}Na^+$ Calcd 822.2746; Selected signals $^1$H NMR (DMSO-$d_6$)[56] δ 6.47 (d, 1H, ex, $J$ = 3.7 Hz, 3′-$OH_B$), 6.43 (d, 1.4H, ex, $J$ = 3.8 Hz, 3′-$OH_A$), 6.25 (s, 1H, H-1′$_B$), 5.80 (s, 1.4H, H-1′$_A$), 4.79 (d, 1H, $J$ = 3.7 Hz, H-3′$_B$), 4.56 (d, 1.4H, $J$ = 3.8 Hz, H-3′$_A$), 2.05 (s, 4.2H, $CH_{3\text{-}A}$), 1.92 (s, 3H, $CH_{3\text{-}A}$); $^{13}$C NMR (DMSO-$d_6$) $\delta$ 169.6, 169.5, 164.2, 163.8, 158.3, 158.1, 150.3, 149.6, 144.8, 144.6, 135.4, 135.3, 135.2, 135.1, 134.6, 131.6, 131.4, 130.7, 130.5, 130.25, 130.18, 129.9, 129.8, 128.8, 128.53, 128.46, 128.1, 127.9, 127.8, 127.7, 127.3, 127.2, 126.92, 126.86, 126.8, 126.4, 126.2, 126.1, 125.9, 124.9, 124.5, 124.2, 123.8, 123.7, 123.6, 113.4, 113.2, 109.1, 108.5, 89.0, 88.8, 86.0, 85.6, 85.4, 72.4, 71.5, 64.9, 62.0, 60.3, 59.6, 55.1, 55.0, 53.9, 52.1, 12.6, 12.5; Anal. Calc. for $C_{49}H_{41}N_3O_8{\cdot}1\ H_2O$: C, 71.96; H, 5.30; N, 5.14; Found: C, 71.63; H, 4.95; N, 4.77.

### (1*S*,3*R*,4*S*,7*R*)-7-[2-Cyanoethoxy(diisopropylamino)phosphinoxy]-1-(4,4′-dimethoxytrityloxymethyl)-5-ethyl-3-(thymin-1-yl)-2-oxa-5-azabicyclo[2.2.1]heptane 3S

Nucleoside **2S** (190 mg, 0.32 mmol) was coevaporated with anhydrous 1,2-dichloroethane (2 × 5 mL) and dissolved in a mixture of anhydrous EtN(*i*-Pr)$_2$ in $CH_2Cl_2$ (2 mL, 20%, v/v). To this was added 2-cyanoethyl *N*,*N*′-(diisopropyl)phosphoramidochloridite (0.14 mL, 0.63 mmol) and the reaction mixture was stirred at rt for 1 h, whereupon it was diluted with $CH_2Cl_2$ (20 mL). The organic phase was washed with sat. aq. $NaHCO_3$ (10 mL) and the aqueous phase back-extracted with $CH_2Cl_2$ (25 mL). The combined organic phase was evaporated to dryness and the resulting residue purified by silica gel column chromatography (0-50% EtOAc in petroleum ether, v/v) to afford amidite **3S** (160 mg, 63%) as a white solid material. $R_f$ = 0.5 (70% EtOAc in petroleum ether, v/v); MALDI-HRMS *m/z* 822.3636 ([M + Na]$^+$, $C_{43}H_{54}N_5O_8P{\cdot}Na^+$ Calcd 822.3602); $^{31}$P NMR ($CH_3CN$ + DMSO-$d_6$) $\delta$ 149.8, 147.9.

### (1*S*,3*R*,4*S*,7*R*)-7-[2-Cyanoethoxy(diisopropylamino)phosphinoxy]-1-(4,4′-dimethoxytrityloxymethyl)-5-(pyren-1-yl)carbonyl-3-(thymin-1-yl)-2-oxa-5-azabicyclo[2.2.1]heptane 3X

Nucleoside **2X** (0.31 g, 0.39 mmol) was dried by coevaporation with anhydrous 1,2-dichloroethane (2 × 5 mL) and dissolved in anhydrous $CH_2Cl_2$ (10 mL). To this was added *N*,*N*′-diisopropylammonium tetrazolide (112 mg, 0.66 mmol) and bis(*N*,*N*′-diisopropylamino)-2-cyanoethoxyphosphine (0.21 mL, 0.66 mmol) and the reaction mixture was stirred at rt for 12 h, whereupon it was diluted with $CH_2Cl_2$ (20 mL), washed with sat. aq. $NaHCO_3$ (10 mL) and brine (10 mL). The aqueous phase was back extracted with $CH_2Cl_2$ (30 mL) and the combined organic phase was evaporated to dryness and the resulting residue purified by silica gel column chromatography (0-50% acetone in petroleum ether, v/v) to afford amidite **3X** as a white solid material (276 mg, 71%). $R_f$ = 0.5 (50% acetone in petroleum ether, v/v); MALDI-HRMS *m/z* 1022.3864 ([M + Na]$^+$, $C_{58}H_{58}N_5O_9PNa^+$ Calcd. 1022.3852; $^{31}$P NMR ($CH_3CN$ + DMSO-$d_6$) $\delta$ 154.2, 153.8, 153.3, 151.9.

### Protocol for synthesis of ONs

ONs containing 2′-amino-α-L-LNA monomers **Q**-**Z** (see Fig. 1 for structures) were synthesized on a 0.2 μmol scale using succinyl linked LCAA-CPG (long chain alkyl amine controlled pore glass) columns with a pore size of 500 Å on an automated DNA synthesizer. Synthesis of α-L-LNA and 2′-amino-α-L-LNA was performed as previously described.[15b,24b] For the incorporation of the N2′-functionalized 2′-amino-α-L-LNA monomers (**S**-**Z**), standard procedures were used, i.e., trichloroacetic acid in $CH_2Cl_2$ as a detrytilation reagent; 0.25 M 4,5-dicyanoimidazole (DCI) in $CH_3CN$ as activator; acetic anhydride in THF as cap A solution;

1-methylimidazole in THF as cap B solution, and 0.02 M iodine in $H_2O$/pyridine/THF as the oxidizing solution. Extended coupling times were used for phosphoramidites **3S** (10 min), **3V** (10 min), **3W** (30 min), **3Y** (30 min), **3X** (30 min), **3Z** (15 min) using 1*H*-tetrazole as catalyst resulted in stepwise coupling yields of ~99% for monomers **S, V, X, Y, Z** and ~95% for monomer **W**. Coupling yields were determined by trityl monitoring. Removal of the nucleobase protecting groups of ONs and cleavage from solid support was accomplished using standard conditions (32% aq. ammonia for 12-16 h at 55 °C). Unmodified DNA and RNA strands were obtained from commercial suppliers and, if necessary, further purified as described below.

Purification of all modified ONs (till minimum 80% purity) was performed by two different methods: a) if overall yield > 90%: precipitation of crude ONs (DMT-OFF, abs. EtOH, −18 °C, 12-16 h, followed by washing with abs. EtOH (2 × 300 μL), b) purification of the ONs (DMT-ON) by RP-HPLC using the system described below, followed by detritylation (80% aq. AcOH, 20 min, rt) and precipitation/washing as outlined above. Purification of crude ONs (DMT-ONs) was performed using a HPLC system equipped with an Xterra MS C18 (10μm, 7.8×10mm) pre-column and an Xterra MS C18 (10μm, 7.8×150mm) column using the representative gradient protocol depicted in Table S1. The composition of all synthesized ONs were verified by MALDI-MS analysis (Table S3) recorded in negative ion mode using 3-hydroxypicolinic acid as a matrix, whereas the purity (>80%) was verified by ion-exchange HPLC system equipped with a Dionex PA100 column (4 × 250 mm) at pH 8 using the representative protocol shown in Table S2.

## Protocol thermal denaturation studies

Concentrations of ONs were estimated using the following extinction coefficients for DNA (OD/μmol): G (12.01), A (15.20), T (8.40), C (7.05); for RNA (OD/μmol): G (13.70), A (15.40), U (10.00), C (9.00); and for pyrene (22.4). ONs (1.0 μM each strand) were thoroughly mixed, denatured by heating and subsequently cooled to the starting temperature of the experiment. Quartz optical cells with a pathlength of 1.0 cm were used. Thermal denaturation temperatures ($T_m$ values/°C) were measured on a UV/VIS spectrometer equipped with a Peltier temperature programmer and determined as the maximum of the first derivative of the thermal denaturation curve ($A_{260}$ vs. temperature) recorded in medium salt buffer ($T_m$-buffer; 100 mM NaCl, 0.1 mM EDTA and pH 7.0 adjusted with 10 mM $NaH_2PO_4$/5 mM $Na_2HPO_4$). For studies evaluating the dependence of $T_m$ on ionic strength, $T_m$ values were also determined in low and high salt buffers (composition as for medium salt buffer except that 0 mM and 700 mM NaCl were used, respectively). The temperature of the denaturation experiments ranged from at least 15 °C below $T_m$ to 20 °C above $T_m$ (although not below 1 °C). A temperature ramp of 1.0 °C/min was used in all experiments. Reported thermal denaturation temperatures are an average of two measurements within ±1.0 °C.

## Protocol for determination of thermodynamic parameters

Thermodynamic parameters were obtained by analysis of the melting curves used to determine $T_m$ values assuming bimolecular reactions and two state equilibrium hypothesis, using software accompanying the utilized UV/VIS spectrometer. The graphs of ln $K_a$ (affinity constant) as a function of 1/T were approximated with straight lines facilitating parameter determination (ΔG, ΔH and ΔS, Tables 4 and 5). Quality of the baseline permitting, thermodynamic parameters for two melting curves per investigated duplex were determined, and an average value was listed. The changes in Gibbs free energy, ΔG, were determined at temperatures close to the $T_m$-value of the investigated duplexes to minimize errors ($T$ = 298 K).

## Supplementary Material

Refer to Web version on PubMed Central for supplementary material.

## Acknowledgments

We greatly appreciate financial support from Idaho NSF EPSCoR, the BANTech Center at the University of Idaho, a University of Idaho Research Office and Research Council Seed Grant, NIH Grant Number P20 RR016448 from the COBRE Program of the National Center for Research Resources, and The Danish National Research Foundation. The Ph.D. school Nucleic Acid Based Drug Design (NAC DRUG) supported by the Danish Agency for Science Technology and Innovation is gratefully acknowledged. The Hrdlicka research team is thanked for proof-reading of the manuscript preparation.

## References and Footnotes

‖A research center funded by the Danish National Research Foundation for studies on nucleic acid chemical biology.

1. a Duca M, Vekhoff P, Oussedik K, Halby L, Arimondo PB. Nucleic Acids Res 2008;36:5123–5138. [PubMed: 18676453] b Simon P, Cannata F, Concordet J-P, Giovannangeli C. Biochimie 2008;90:1109–1116. [PubMed: 18460344] c Kurreck J. Eur. J. Biochem 2003;270:1628–1644. [PubMed: 12694176] d Corey DR. J. Clin. Invest 2007;117:3615–3622. [PubMed: 18060019] e Watts JK, Deleavey GF, Damha MJ. Drug Disc. Today 2008;13:842–855.
2. a Asseline U. Curr. Opin. Chem 2006;10:491–518. b Ranasinghe RT, Brown T. Chem. Commun 2005:5487–5502.
3. For representative reviews see: a Wengel J. Org. Biomol. Chem 2004;2:277–280. [PubMed: 14747851] , b Gothelf KV, LaBean TH. Org. Biomol. Chem 2005;3:4023–4037. [PubMed: 16267576] , c Clever GH, Kaul C, Carell T. Angew. Chem. Int. Ed 2007;46:6226–6236.
4. For reviews see a Meldgaard M, Wengel J. J. Chem. Soc. Perkin Trans. 1 2000:3539–3554., b Leumann CJ. Bioorg. Med. Chem 2002;10:841–854. [PubMed: 11836090]
5. For recent representative examples see a Morita K, Takagi M, Hasegawa C, Kaneko M, Tsutsumi S, Sone J, Ishikawa T, Imanishi T, Koizumi M. Bioorg. Med. Chem 2003;11:2211–2226. [PubMed: 12713831] , b Albæk N, Petersen M, Nielsen P. J. Org. Chem 2006;71:7731–7740. [PubMed: 16995680] , c Honcharenko D, Vargese OP, Plashkevych O, Barman J, Chattopadhyaya J. J. Org. Chem 2006;71:299–314. [PubMed: 16388649] , d Varghese OP, Barman J, Pathmasiri W, Plaskevych O, Honcharenko D, Chattopadhyaya J. J. Am . Chem. Soc 2006;128:15173–15187. [PubMed: 17117869] , e Hari Y, Obika S, Ohnishi R, Eguchi K, Osaki T, Ohishi H, Imanishi T. Bioorg. Med. Chem 2006;14:1029–1038. [PubMed: 16213732] , f Plashkevych O, Chatterjee S, Honcharenko D, Pathmasiri W, Chattopadhyaya J. J. Org. Chem 2007;72:4716–4726. [PubMed: 17523663] , g Srivastava P, Barman J, Pathmasiri W, Plaskevych O, Wenska M, Chattopadhyaya J. J. Am. Chem. Soc 2007;129:8362–8379. [PubMed: 17552524] , h Sabatino D, Damha MJ. J. Am. Chem. Soc 2007;129:8259–8270. [PubMed: 17559214] , i Abdur Rahman SM, Seki S, Obika S, Yoshikawa H, Miyashita K, Imanishi T. J. Am. Chem. Soc 2008;130:4886–4896. [PubMed: 18341342] , j Enderlin G, Nielsen P. J. Org. Chem 2008;73:6891–6894. [PubMed: 18672932]
6. We define LNA, *α*-L-LNA, 2′-amino-LNA and 2′-amino-*α*-L-LNA as a oligonucleotide containing one or more 2′-*O*,4′-*C*-methylene-*β*-D-ribofuranosyl monomer(s), 2′-*O*,4′-*C*-methylene-*α*-L-ribofuranosyl monomer(s), 2′-amino-2′-deoxy-2′-*N*,4′-*C*-methylene-*β*-D-ribofuranosyl monomer(s) or 2′-amino-2′-deoxy-2′-*N*,4′-*C*-methylene-*α*-L-ribofuranosyl monomer(s), respectively. Similar definitions are used for N2′-functionalized *α*-L-LNA derivatives.
7. a Singh SK, Nielsen P, Koshkin AA, Wengel J. Chem. Commun 1998:455–456. b Koshkin AA, Singh SK, Nielsen P, Rajwanshi VK, Kumar R, Meldgaard M, Olsen CE, Wengel J. Tetrahedron 1998;54:3607–3630. c Wengel J. Acc. Chem. Res 1999;32:301–310.
8. Obika S, Nanbu D, Hari Y, Andoh J, Morio K, Doi T, Imanishi T. Tetrahedron Lett 1998;39:5401–5404.
9. Petersen M, Wengel J. Trends Biotechnol 2003;21:74–81. [PubMed: 12573856]
10. Kaur H, Babu BR, Maiti S. Chem. Rev 2007;107:4672–4697. [PubMed: 17944519]

11. Jepsen JS, Wengel J. Curr. Opin. Drug Discovery Dev 2004;7:188–194.
12. Frieden M, Ørum H. IDrugs 2006;9:706–711. [PubMed: 17016778]
13. Grünweller A, Hartmann RK. Biodrugs 2007;21:235–243. [PubMed: 17628121]
14. Stenvang J, Silahtaroglu AN, Lindow M, Elmen J, Kauppinen S. Sem. Cancer Biol 2008;18:89–102.
15. a Rajwanshi VK, Håkansson AE, Dahl BM, Wengel J. Chem. Commun 1999:1395–1396. b Sørensen MD, Kværnø L, Bryld T, Håkansson AE, Verbeure B, Gaubert G, Herdewijn P, Wengel J. J. Am. Chem. Soc 2002;124:2164–2176. [PubMed: 11878970]
16. Arzumanov A, Stetsenko DA, Malakhov AD, Techelt S, Sørensen MD, Babu BR, Wengel J, Gait MJ. Oligonucleotides 2003;13:435–453. [PubMed: 15025911]
17. Frieden M, Christen SM, Mikkelsen ND, Rosenbohm C, Thrue CA, Westergaard M, Hansen HF, Ørum H, Koch T. Nucleic Acids Res 2003;31:6365–6372. [PubMed: 14576324]
18. Fluiter K, Frieden M, Vreijling J, Rosenbohm C, De Wissel MB, Christensen SM, Koch T, Ørum H, Baas F. ChemBioChem 2005;6:1104–1109. [PubMed: 15861430]
19. Kumar N, Nielsen KE, Maiti S, Petersen M. J. Am. Chem. Soc 2006;128:14–15. [PubMed: 16390098]
20. Vester B, Hansen LH, Lundberg LB, Babu BR, Sørensen MD, Wengel J, Doubtwaite S. BMC Mol. Biol 2006;7:19. [PubMed: 16753066]
21. Crinelli R, Bianchi M, Gentilini L, Palma L, Sørensen MD, Bryld T, Babu BR, Arar K, Wengel J, Magnani M. Nucleic Acids Res 2004;32:1874–1885. [PubMed: 15051810]
22. Singh SK, Kumar R, Wengel J. J. Org. Chem 1998;63:10035–10039.
23. a Sørensen MD, Petersen M, Wengel J. Chem. Commun 2003:2130–2131. b Hrdlicka PJ, Babu BR, Sørensen MD, Wengel J. Chem. Commun 2004:1478–1479. c Babu BR, Hrdlicka PJ, McKenzie CJ, Wengel J. Chem. Commun 2005:1705–1707. d Hrdlicka PJ, Babu BR, Sørensen MD, Harrit N, Wengel J. J. Am. Chem. Soc 2005;127:13293–13299. [PubMed: 16173760] e Lindegaard D, Babu BR, Wengel J. Nucleosides Nucleotides Nucleic Acids 2005;24:679–681. [PubMed: 16248013] f Bramsen JB, Laursen MB, Damgaard CK, Lena SW, Babu BR, Wengel J, Kjems J. Nucleic Acids Res 2007;35:5886–5897. [PubMed: 17726057] g Kalek M, Madsen AS, Wengel J. J. Am. Chem. Soc 2007;129:9392–9400. [PubMed: 17616191] h Umemoto T, Hrdlicka PJ, Babu BR, Wengel J. ChemBioChem 2007;8:2240–2248. [PubMed: 17979173] i Lindegaard D, Madsen AS, Astakhova IV, Malakhov AD, Babu BR, Korshun VA, Wengel J. Bioorg. Med. Chem 2008;16:94–99. [PubMed: 17920888] j Kalek M, Benediktson P, Vester B, Wengel J. Chem. Commun 2008:762–764.Østergaard, ME.; Maity, J.; Wengel, J.; Hrdlicka, PJ. Abstracts of Papers, 235th ACS National Meeting; New Orleans. 2008; BIOL-032
24. a Hrdlicka PJ, Kumar TS, Wengel J. Nucleosides Nucleotides Nucleic Acids 2005;24:1101–1104. [PubMed: 16248100] b Kumar TS, Madsen AS, Wengel J, Hrdlicka PJ. J. Org. Chem 2006;71:4188–4201. [PubMed: 16709060]
25. a Hrdlicka PJ, Kumar TS, Wengel J. Chem. Commun 2005:4279–4281. b Kumar TS, Wengel J, Hrdlicka PJ. ChemBioChem 2007;8:1122–1125. [PubMed: 17551917] c Andersen NK, Wengel J, Hrdlicka PJ. Nucleosides Nucleotides Nucleic Acids 2007;26:1415–1417. [PubMed: 18066795] d Kumar TS, Madsen AS, Østergaard ME, Wengel J, Hrdlicka PJ. J. Org. Chem 2008;73:7060–7066. [PubMed: 18710289]
26. Preliminary results have been briefly outlined in Kumar TS, Madsen AS, Wengel J, Hrdlicka PJ. Nucleosides Nucleotides Nucleic Acids 2007;26:1403–1405. [PubMed: 18066792]
27. Abdel-Magid AF, Carson KG, Harris BD, Maryanoff CA, Shah RD. J. Org. Chem 1996;61:3849–3862. [PubMed: 11667239]
28. Pedersen DS, Rosenbohm C, Koch T. Synthesis 2002:802–808.
29. See Supporting information.
30. a Christensen UB, Pedersen EB. Nucleic Acids Res 2002;30:4918–4925. [PubMed: 12433995] b Filichev VV, Hilmy KMH, Christensen UB, Pedersen UB. Tetrahedron Lett 2004;45:4907–4910.
31. Yamana K, Iwase R, Furutani S, Tsuchida H, Zako H, Yamaoka T, Murakami A. Nucleic Acids Res 1999;27:2387–2392. [PubMed: 10325429]
32. Bryld T, Højland T, Wengel J. Chem. Comm 2004:1064–1065. [PubMed: 15116186]
33. Nielsen KME, Petersen M, Håkansson AE, Wengel J, Jacobsen JP. Chem. Eur. J 2002;8:3001–3009.

34. a Weiner SJ, Kollman PA, Case DA, Singh UC, Ghio C, Alagona G, Profeta S, Weiner P. J. Am. Chem. Soc 1984;106:765–784. b Weiner SJ, Kollman PA, Nguyen DT, Case DA. J. Comp. Chem 1986;7:230–252.
35. Still WC, Tempczyk A, Hawley RC, Hendrickson T. J. Am. Chem. Soc 1990;112:6127–6129.
36. MacroModel version 9.1. S., LLC; New York, NY: 2005.
37. Egli M, Tereshko V, Teplova M, Minasov G, Joachimiak A, Sanishvili R, Weeks CM, Miller R, Maier MA, An H, Cook PD, Manoharan M. Biopolymers 1998;48:234–252. [PubMed: 10699842]
38. Kielkopf CL, Ding S, Kuhn P, Rees DC. J. Mol. Biol 2000;296:787–801. [PubMed: 10677281]
39. a Korshun VA, Stetsenko DA, Gait MJ. J. Chem. Soc. Perkin Trans. 1 2002:1092–1104. b Dioubankova NN, Malakhov AD, Stetsenko DA, Gait MJ, Volynsky PE, Efremov RG, Korshun VA. ChemBioChem 2003;4:841–847. [PubMed: 12964158] c Kalra N, Babu BR, Parmar VS, Wengel J. Org. Biomol. Chem 2004;2:2885–2887. [PubMed: 15480448] d Donho C, Saito I. ChemBioChem 2005;6:1075–1081. [PubMed: 15852333]
40. Nakamura M, Fukunaga Y, Sasa K, Ohtoshi Y, Kanaori K, Hayashi H, Nakano H, Yamana K. Nucleic Acids Res 2005;33:5887–5895. [PubMed: 16237124]
41. Dougherty G, Pilbrow JR. Int. J. Biochem 1984;16:1179–1192. [PubMed: 6397369]
42. Okamoto A, Kanatani K, Saito I. J. Am. Chem. Soc 2004;126:4820–4827. [PubMed: 15080686]
43. a Wang AH-J, Ughetto G, Quigley GJ, Rich A. Biochemistry 1987;26:1152–1163. [PubMed: 3567161] b Spielmann HP, Wemmer DE, Jacobsen JP. Biochemistry 1995;34:8542–8553. [PubMed: 7612596] c Gallego J, Reid BR. Biochemistry 1999;38:15104–15115. [PubMed: 10563793] d Mukherjee A, Lavery R, Bagchi B, Hynes JT. J. Am. Chem. Soc 2008;130:9747–9755. [PubMed: 18611009]
44. Following definitions of torsion angles are used: $\chi$ (O4′-C1′-N1-C2 or O4′-C1′-N9-C4 for pyrimidines or purines, respectively). The pseudorotation phase angle $P$ is given as tan $P = (\nu_4+\nu_1)-\nu_3+\nu_0) / [2\nu_2 (\sin 36° + \sin 72°)]$, where $\nu_0$ (C4′-O4′-C1′-C2′),$\nu_1$ (O4′-C1′-C2′-C3′), $\nu_2$ (C1′-C2′-C3′-C4′), $\nu_3$ (C2′-C3′-C4′-O4′) and $\nu_4$ (C3′-C4′-O4′-C1′). For further information see Saenger, W. Principles of Nucleic Acid Structure. Springer-Verlag; Berlin: 1984.
45. Afonina I, Kutyavin I, Lukhtanov E, Meyer RB, Gamper H. Proc. Natl. Acad. Sci. USA 1996;93:3199–3204. [PubMed: 8622913]
46. Kutyavin IV, Afonina IA, Mills A, Gorn VV, Lukhtanov EA, Belousov ES, Singer MJ, Walburger DK, Lokhov SG, Gall AA, Dempcy R, Reed MW, Meyer RB, Hedgpeth J. Nucleic Acids Res 2000;28:655–661. [PubMed: 10606668]
47. Persil Ö, Hud NV. Trends Biotechnol 2007;25:433–436. [PubMed: 17825446]
48. Wilson JN, Kool ET. Org. Biomol. Chem 2006;4:4265–4274. [PubMed: 17102869]
49. Köhler O, Jarikote DV, Seitz O. ChemBioChem 2005;6:69–77. [PubMed: 15584015]
50. Benvin AL, Creeger Y, Fisher GW, Ballou B, Wagonner AS, Armitage BA. J. Am. Chem. Soc 2007;129:2025–2034. [PubMed: 17256855]
51. Shao F, Augustyn K, Barton JK. J. Am. Chem. Soc 2005;127:17445–17452. [PubMed: 16332096]
52. Clever GH, Kaul C, Carell T. Angew. Chem. Int. Ed 2007;46:6226–6236.
53. Tanaka K, Shionoya M. Coord. Chem. Rev 2007;251:2732–2742.
54. Nakano S-I, Uotani Y, Uenishi K, Fujii M, Sugimoto N. J. Am. Chem. Soc 2005;127:518–519. [PubMed: 15643864]
55. Assignments of $^{1}$H NMR signals of H5′ and H5″ (and of the corresponding $^{13}$C signals) may in principle be interchanged.
56. The integral of the H1′-signal of the least predominant rotamer (termed B) is set to 1.0.

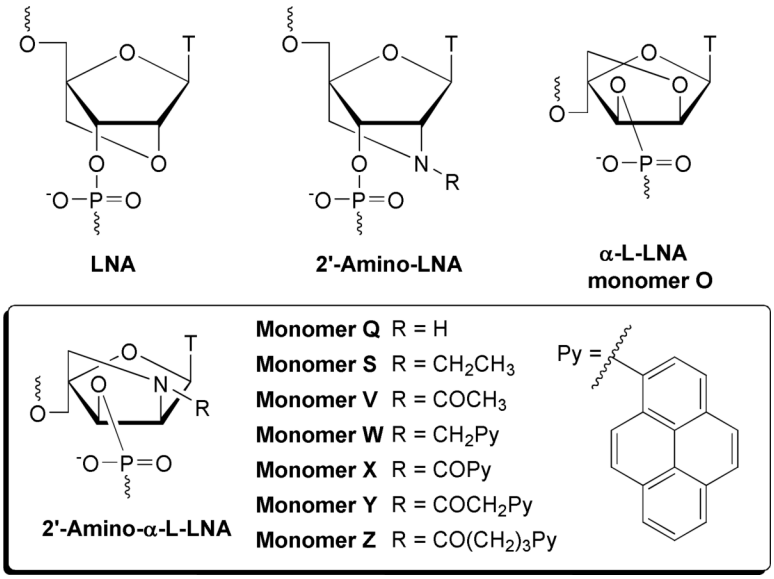


**Figure 1.**
Structures of LNA, 2′-Amino-LNA, α-L-LNA (monomer **O**), and 2′-Amino-α-L-LNA monomers **Q**-**Z**.

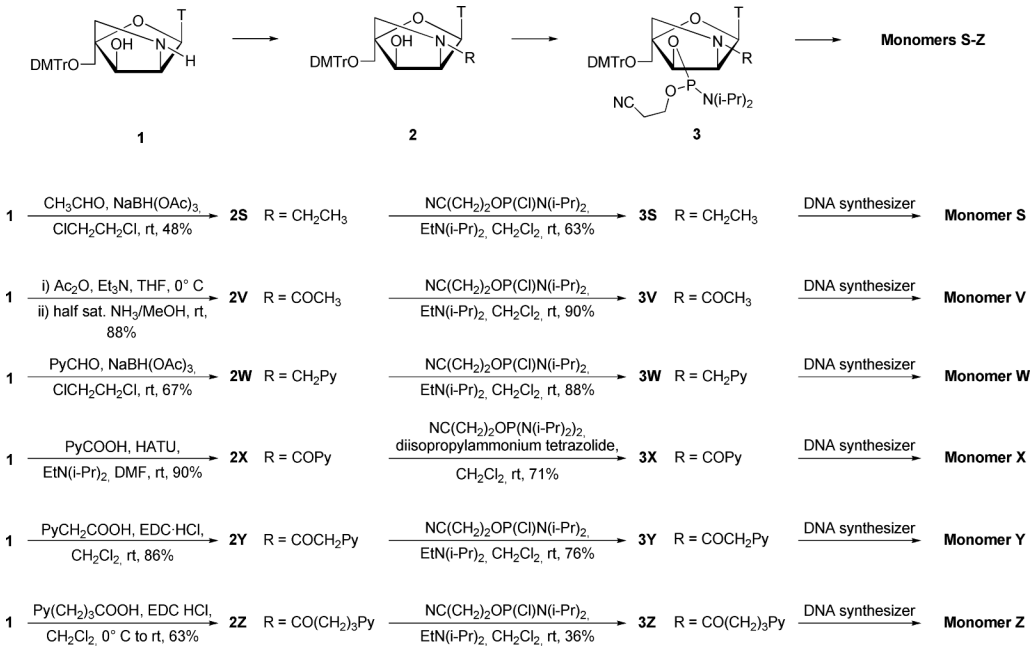


**Scheme 1.**

Synthesis of N2′-functionalized 2′-amino-α-L-LNA phosphoramidites. DMTr = 4,4′-dimethoxytrityl, T = thymin-1-yl, Py = pyren-1-yl, EDC·HCl = 1-ethyl-3-(3-dimethylaminopropyl)-carbodiimide hydrochloride, HATU = *O* (7-Azabenzotriazole-1-yl)-*N*,*N*,*N*′,*N*′-tetramethyluronium hexafluorophosphate.

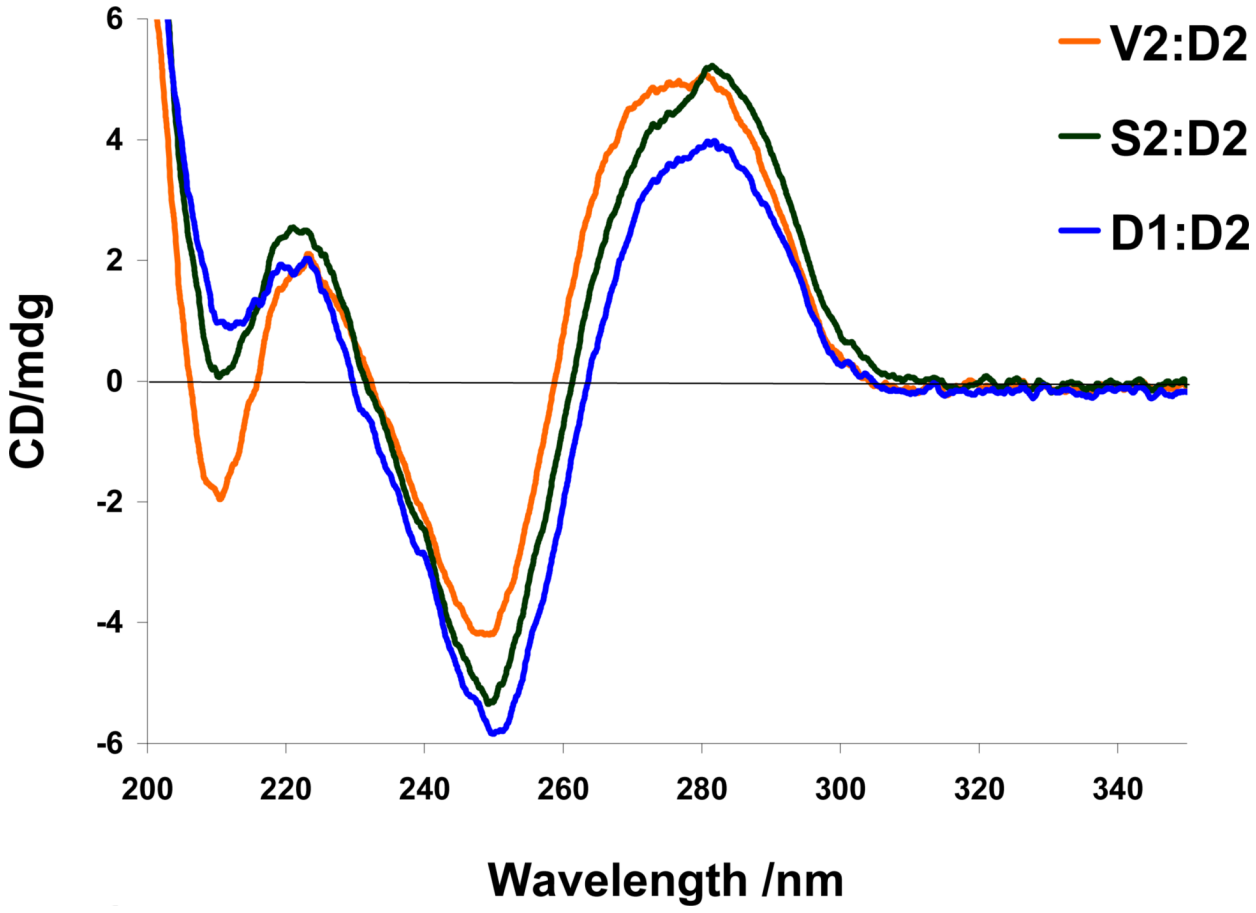


**Figure 2.**
Circular dichroism spectra of **D1:D2, S2:D2** and **V2:D2**.

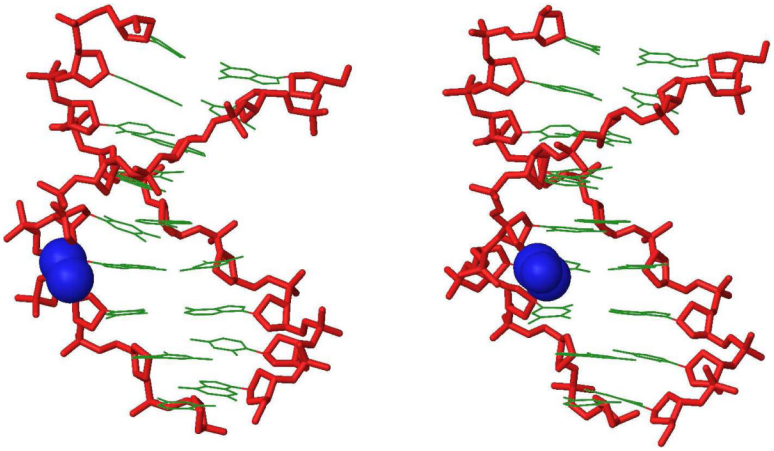

**Figure 3.**

Side view representations of the lowest energy structure of **S2:D2** (left) and **V2:D2** (right). For clarity, hydrogen atoms, sodium ions and bond orders have been omitted. Coloring scheme: nucleobases, green; sugar-phosphate backbone, red; ethyl moiety of monomer **S** and acetyl moiety of monomer **V**, blue.

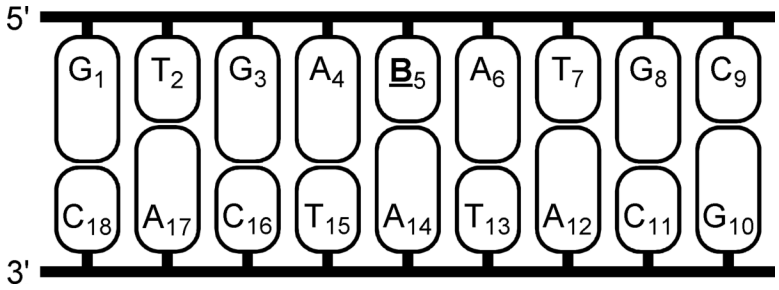


**Figure 4.**
Nucleotide numbering for duplexes studied by molecular modeling; **B** = thymidine (**D1**) or monomers **O-Z** (**O2-Z2**).

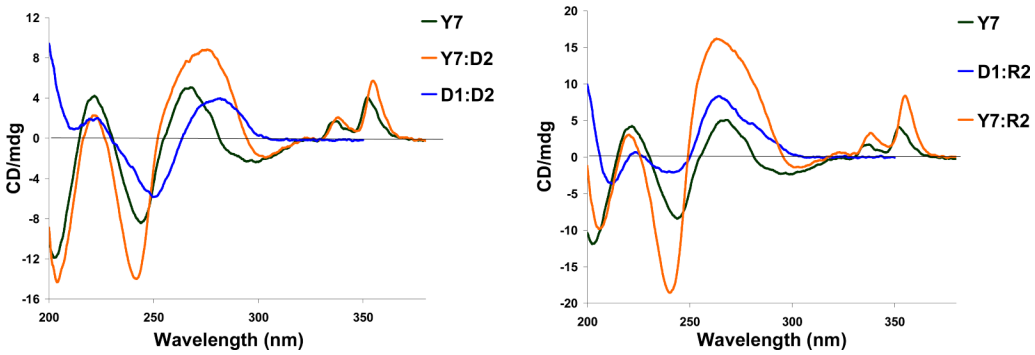


**Figure 5.**
Circular dichroism spectra of **Y7** (5′-GYG AYA YGC) and its duplexes with DNA/RNA complements, and reference DNA:DNA (**D1:D2**) and DNA:RNA (**D1:R2**).

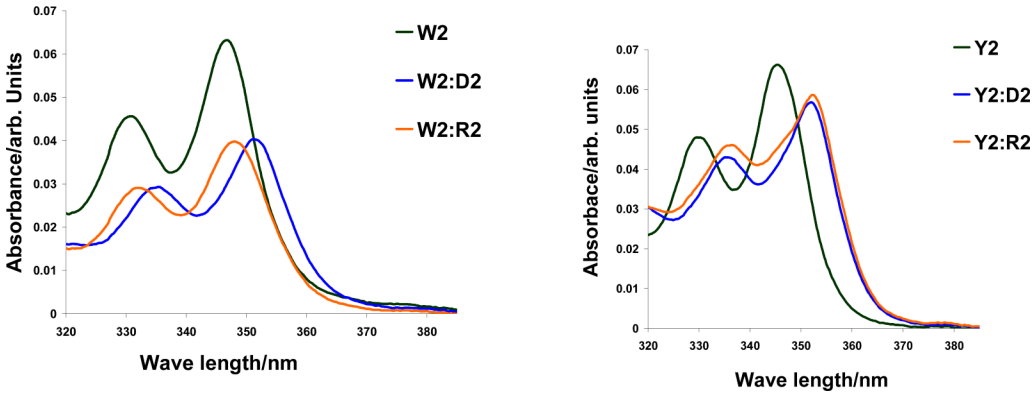


**Figure 6.**
Absorption spectra of **W2** (left panel) and **Y2** (right panel) and their duplexes with complementary DNA (**D2**) and RNA (**R2**) targets.

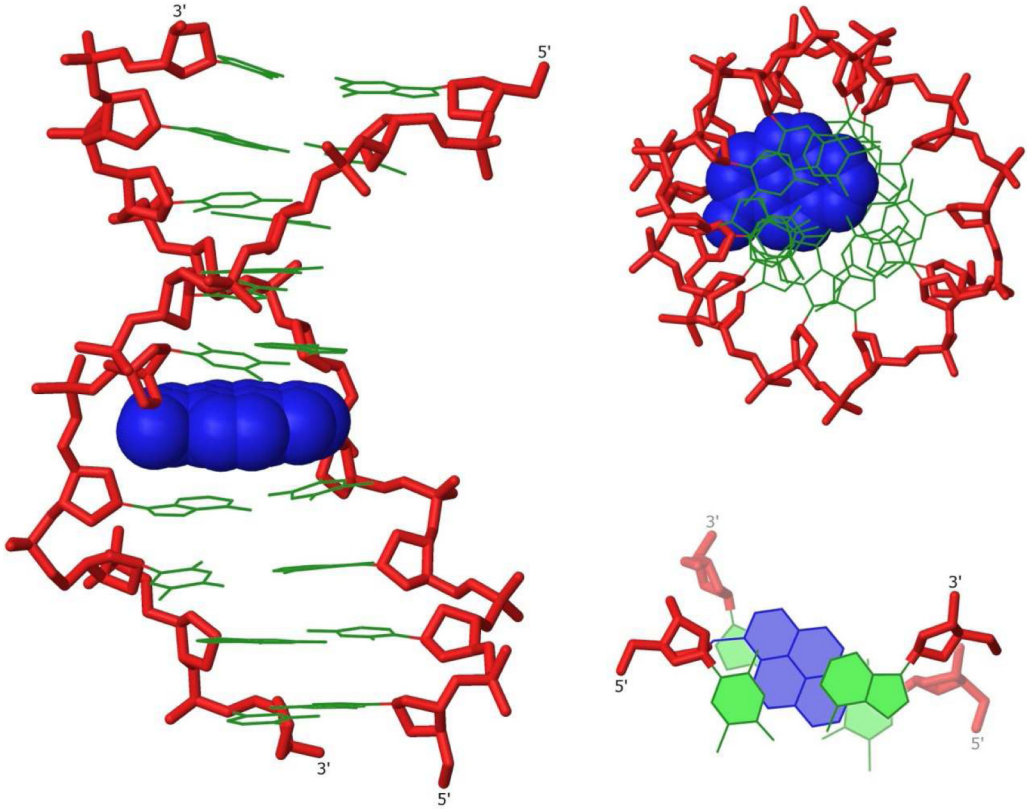


**Figure 7.**

Three representations of the lowest energy structure of **W2:D2**, side view (left), top view (upper right) and truncated top view showing $\mathbf{W_5A_6{:}T_{13}A_{14}}$ (lower right). Coloring scheme as in Fig. 3 except that pyren-1-yl-methyl moiety of monomer **W** is in blue.

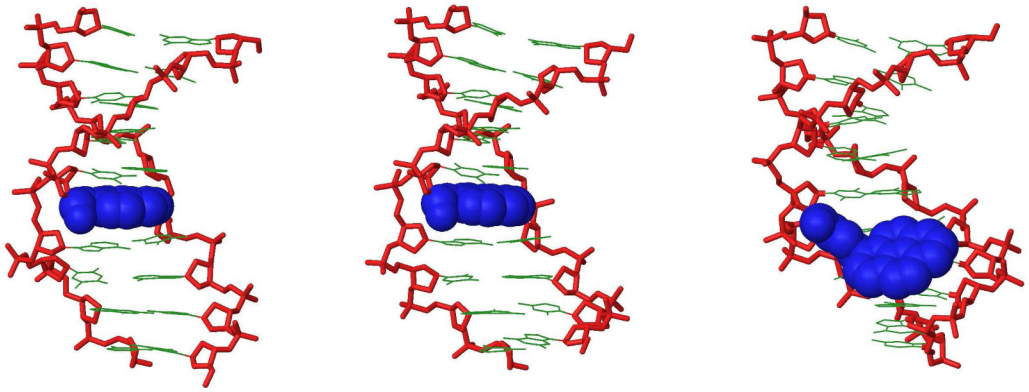

**Figure 8.**

Side view representations of the lowest energy structures of **X2:D2, Y2:D2** and **Z2:D2** (non-intercalated binding mode), respectively. Coloring scheme as in Fig. 3 except that pyrene moieties are shown in blue.

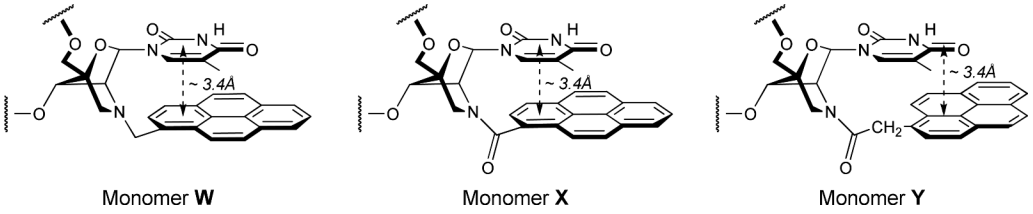


**Figure 9.**
Illustration of directed positioning of pyrene moieties in duplex core by N2′-functionalized 2′-amino-α-L-LNA.

**Table 1**

Thermal denaturation data for N2′-Functionalized 2′-amino-α-L-LNA and reference strands against DNA complements.[a]

| | | | $T_m$ [$\Delta T_m$/mod] (°C) | | | | | | | | |
|---|---|---|---|---|---|---|---|---|---|---|---|
| **ON** | **Duplex** | **B =** | **T** | **O** | **Q** | **S** | **V** | **W** | **X** | **Y** | **Z** |
| **B1** | 5′-G**B**G ATA TGC | | 28.5 | 31.0 | 26.5 | 20.0 | 17.5 | 35.5 | 38.5 | 39.0 | 29.0 |
| **D2** | 3′-CAC TAT ACG | | | [+2.5] | [–2.0] | [–8.5] | [–11.0] | [+7.0] | [+10.0] | [+10.5] | [+0.5] |
| **B2** | 5′-GTG A**B**A TGC | | 28.5 | 34.5 | 29.0 | 20.0 | 16.5 | 42.5 | 47.5 | 44.0 | 34.5 |
| **D2** | 3′-CAC TAT ACG | | | [+6.0] | [+0.5] | [–8.5] | [–12.0] | [+14.0] | [+19.0] | [+15.5] | [+6.0] |
| **B3** | 5′-GTG ATA **B**GC | | 28.5 | 31.5 | 27.5 | 16.5 | 14.5 | 39.0 | 42.5 | 40.0 | ND |
| **D2** | 3′-CAC TAT ACG | | | [+3.0] | [–1.0] | [–12.0] | [–14.0] | [+10.5] | [+14.0] | [+11.5] | |
| **D1** | 5′-GTG ATA TGC | | 28.5 | 32.0 | 28.0 | 17.0 | 12.0 | 35.0 | 39.0 | 38.5 | 29.0 |
| **B4** | 3′-CAC **B**AT ACG | | | [+3.5] | [–0.5] | [–11.5] | [–16.5] | [+6.5] | [+10.5] | [+10.0] | [+0.5] |
| **D1** | 5′-GTG ATA TGC | | 28.5 | 36.5 | 31.0 | 22.5 | 19.0 | 44.0 | 48.0 | 45.0 | 35.0 |
| **B5** | 3′-CAC TA**B** ACG | | | [+8.0] | [+2.5] | [–6.0] | [–9.5] | [+15.5] | [+19.5] | [+16.5] | [+6.5] |
| **D1** | 5′-GTG ATA TGC | | 28.5 | 36.0 | 27.5 | <10 | <10 | ND | 53.5 | 55.5 | ND |
| **B6** | 3′-CAC **B**A**B** ACG | | | [+3.8] | [–0.5] | | | | [+12.5] | [+13.5] | |
| **B7** | 5′-G**B**G A**B**A **B**GC | | 28.5 | 36.0 | 27.0 | <10 | <10 | ND | ND | 69.0 | ND |
| **D2** | 3′-CAC TAT ACG | | | [+2.5] | [–0.5] | | | | | [+13.5] | |

[a] Thermal denaturation temperatures [$T_m$ values/°C ($\Delta T_m$ = change in $T_m$ value calculated relative to **D1:D2, D1:R2** and **R1:D2** reference duplexes)] measured as the maximum of the first derivative of the melting curve ($A_{260}$ vs temperature) recorded in medium salt buffer ([$Na^+$] = 110 mM, [$Cl^-$] = 100 mM, pH 7.0 ($NaH_2PO_4/Na_2HPO_4$)), using 1.0 μM concentrations of the two complementary strands. $T_m$ values are averages of at least two measurements; A = adenin-9-yl DNA monomer, C = cytosin-1-yl DNA monomer, G = guanin-9-yl DNA monomer, T = thymin-1-yl DNA monomer, **O** = α-L-LNA thymin-1-yl monomer (Fig. 1). For structures of monomers **Q-Z** see Figure 1. ND = not determined.

**Table 2**

Thermal denaturation data for N2′-functionalized 2′-amino-α-L-LNA and reference strands against RNA complements.[a]

| | | | $T_m$ [$\Delta T_m$/mod] (°C) | | | | | | | | |
|---|---|---|---|---|---|---|---|---|---|---|---|
| **ON** | **Duplex** | **B =** | **T** | **O** | **Q** | **S** | **V** | **W** | **X** | **Y** | **Z** |
| **B1** | 5′-G**B**G ATA TGC | | 26.5 | 32.5 | 27.5 | 19.5 | 19.0 | 27.0 | 32.5 | 32.5 | 26.5 |
| **R2** | 3′-CAC UAU ACG | ___ | ___ | [+6.0] | [+1.0] | [–7.0] | [–7.5] | [+0.5] | [+6.0] | [+6.0] | [±0] |
| **B2** | 5′-GTG A**B**A TGC | | 26.5 | 35.0 | 28.5 | 18.5 | 17.0 | 31.5 | 36.5 | 36.0 | 33.5 |
| **R2** | 3′-CAC UAU ACG | ___ | ___ | [+8.5] | [+2.0] | [–8.0] | [–9.5] | [+5.0] | [+10.0] | [+9.5] | [+7.0] |
| **B3** | 5′-GTG ATA **B**GC | | 26.5 | 32.0 | 28.0 | 19.0 | 16.5 | 28.0 | 33.5 | 32.5 | ND |
| **R2** | 3′-CAC UAU ACG | ___ | ___ | [+5.5] | [+1.5] | [–7.5] | [–10.0] | [+1.5] | [+7.0] | [+6.0] | ___ |
| **R1** | 5′-GUG AUA UGC | | 24.5 | 31.0 | 27.5 | 19.5 | 17.5 | 23.5 | 29.0 | 30.5 | 19.5 |
| **B4** | 3′-CAC **B**AT ACG | ___ | ___ | [+6.5] | [+3.0] | [–5.0] | [–7.0] | [–1.0] | [+4.5] | [+6.0] | [–5.0] |
| **R1** | 5′-GUG AUA UGC | | 24.5 | 34.5 | 29.0 | 21.5 | 20.5 | 32.0 | 36.0 | 36.5 | 31.0 |
| **B5** | 3′-CAC TA**B** ACG | ___ | ___ | [+10.0] | [+4.5] | [–3.0] | [–4.0] | [+7.5] | [+11.5] | [+12.0] | [+6.5] |
| **R1** | 5′-GUG AUA UGC | | 24.5 | 35.5 | 28.5 | <10 | <10 | ND | 39.0 | 44.0 | ND |
| **B6** | 3′-CAC **B**A**B** ACG | ___ | ___ | [+5.5] | [+2.0] | ___ | ___ | ___ | [+7.3] | [+9.8] | ___ |
| **B7** | 5′-G**B**G A**B**A **B**GC | | 26.5 | 44.0 | 31.0 | <10 | <10 | ND | ND | 52.5 | ND |
| **D2** | 3′-CAC UAU ACG | | | [+5.8] | [+1.5] | | | | | [+8.7] | |

[a] For conditions of thermal denaturation experiments see Table 1.

**Table 3**

Discrimination of mismatched DNA/RNA targets by N2′-functionalized 2′-amino-α-L-LNA.

| | | | $T_m$ [$\Delta T_m$] (°C) | | | | | | | |
|---|---|---|---|---|---|---|---|---|---|---|
| | | | DNA: 3′-CAC TBT ACG | | | | RNA: 3′-CAC UBU ACG | | | |
| **ON** | **Sequence** | **B =** | **A** | **C** | **G** | **T** | **A** | **C** | **G** | **U** |
| **D1** | 5′-GTG ATA TGC | | **28.5** | 12.0 [–16.5] | 19.0 [–9.5] | 11.5 [–17.0] | **26.5** | <10 [<–16.5] | 22.0 [–4.5] | <10 [<–16.5] |
| **O2** | 5′-GTG A**O**A TGC | | **34.5** | 13.0 [–21.5] | 21.5 [–13.0] | 14.5 [–20.0] | **35.0** | 14.0 [–21.0] | 28.5 [–6.5] | 14.5 [–20.5] |
| **Q2** | 5′-GTG A**Q**A TGC | | **29.0** | <10 [<–19.0] | 17.5 [–11.5] | <10 [<–19.0] | **28.5** | <10 [<–18.5] | 22.5 [–6.0] | <10 [<–18.5] |
| **S2** [b] | 5′-GTG A**S**A TGC | | **28.5** | <10 [<–18.5] | 17.0 [–11.5] | <10 [<–18.5] | **27.0** | <10 [<–17.0] | 25.5 [–1.5] | <10 [<–17.0] |
| **V2** [b] | 5′-GTG A**V**A TGC | | **24.5** | <10 [<–14.5] | 14.5 [–10.0] | <10 [<–14.5] | **24.5** | <10 [<–14.5] | 28.0 [+3.5] | <10 [<–14.5] |
| **W2** | 5′-GTG A**W**A TGC | | **42.5** | 30.0 [–12.5] | 37.0 [–5.5] | 39.0 [–3.5] | **31.5** | 19.5 [–12.0] | 30.5 [–1.0] | 27.0 [–4.5] |
| **X2** | 5′-GTG A**X**A TGC | | **47.5** | 31.0 [–16.5] | 40.0 [–7.5] | 40.5 [–7.0] | **36.5** | 21.0 [–15.5] | 33.5 [–3.0] | 28.5 [–8.0] |
| **Y2** | 5′-GTG A**Y**A TGC | | **44.0** | 26.0 [–18.0] | 38.5 [–5.5] | 34.0 [–10.0] | **36.0** | 14.5 [–21.5] | 33.0 [–3.0] | 25.0 [–11.0] |
| **Z2** | 5′-GTG A**Z**A TGC | | **34.5** | 17.0 [–17.5] | 20.0 [–14.5] | 20.0 [–14.5] | **33.5** | <10 [<–22.5] | 17.5 [–16.0] | <10 [<–22.5] |

[a] For conditions of thermal denaturation experiments see Table 1. $T_m$ values of fully matched duplexes are shown in bold. $\Delta T_m$ = change in $T_m$ value relative to fully matched DNA:DNA or DNA:RNA duplex.

[b] $T_m$ values for duplexes involving **S2** and **V2** are measured using high salt buffer, ([$Na^+$] = 710 mM, [$Cl^-$] = 100 mM, pH 7.0 ($NaH_2PO_4/Na_2HPO_4$)).

**Table 4**

Energetics derived from thermal denaturation curves of duplexes between 2'-amino-α-L-LNA functionalized with non-aromatic moieties and DNA/RNA.[a]

| | | Complementary DNA | | | Complementary RNA | | |
|---|---|---|---|---|---|---|---|
| **ON** | **Sequence** | **$\Delta G^{298}$ [$\Delta\Delta G^{298}$] (kJ/mol)** | **$\Delta H$ [$\Delta\Delta H$] (kJ/mol)** | **$T^{298}\Delta S$ [$\Delta(T^{298}\Delta S)$] (kJ/mol)** | **$\Delta G^{298}$ [$\Delta\Delta G^{298}$] (kJ/mol)** | **$\Delta H$ [$\Delta\Delta H$] (kJ/mol)** | **$T^{298}\Delta S$ [$\Delta(T^{298}\Delta S)$] (kJ/mol)** |
| **D1** | 5′-GTG ATA TGC | –41 | –327 | –286 | –38 | –275 | –237 |
| **O2** | 5′-GTG A**O**A TGC | –46 [–5] | –354 [–27] | –308 [–22] | –46 [–8] | –361 [–86] | –315 [–78] |
| **Q2** | 5′-GTG A**Q**A TGC | *–41 [0]* | *–312 [+15]* | *–271 [+15]* | *–40 [–2]* | *–302 [–27]* | *–261 [–24]* |
| **S2** | 5′-GTG A**S**A TGC | –33 [+8] | –349 [–22] | –316 [–30] | –31 [+7] | –352 [–77] | –321 [–84] |
| **V2** | 5′-GTG A**V**A TGC | *–29 [+12]* | *–295 [+32]* | *–266 [+20]* | –30 [+8] | –303 [–28] | –273 [–36] |

[a] Thermal denaturation curves were obtained as described in Tables 1 and 2. $\Delta\Delta G^{298}$, $\Delta\Delta H$ and $\Delta(T^{298}\Delta S)$ change in $\Delta G^{298}$, $\Delta H$ and $\Delta(T^{298}\Delta S)$ values, respectively, calculated relative to **D1:D2** and **D1:R2** reference duplexes). Values in italics indicate deviation from (or lack of) monomer trend. ND = not determined. See Table S6 for data from **B1-B5** series.

**Table 5**

Energetics derived from thermal denaturation curves of duplexes between N2'-pyrene-functionalized 2'-amino-α-L-LNA and DNA/RNA.[a]

| | | Complementary DNA | | | Complementary RNA | | |
|---|---|---|---|---|---|---|---|
| **ON** | **Sequence** | **$\Delta G^{298}$ [$\Delta\Delta G^{298}$] (kJ/mol)** | **$\Delta H$ [$\Delta\Delta H$] (kJ/mol)** | **$T^{298}\Delta S$ [$\Delta(T^{298}\Delta S)$] (kJ/mol)** | **$\Delta G^{298}$ [$\Delta\Delta G^{298}$] (kJ/mol)** | **$\Delta H$ [$\Delta\Delta H$] (kJ/mol)** | **$T^{298}\Delta S$ [$\Delta(T^{298}\Delta S)$] (kJ/mol)** |
| **D1** | 5′-GTG ATA TGC | –41 | –327 | –286 | –38 | –275 | –237 |
| **W2** | 5′-GTG A**W**A TGC | –53 [–12] | –307 [+20] | –254 [+32] | –44 [–6] | –328 [–53] | –284 [–47] |
| **X2** | 5′-GTG A**X**A TGC | –59 [–18] | –348 [–21] | –289 [–3] | –49 [–11] | –343 [–68] | –294 [–57] |
| **Y2** | 5′-GTG A**Y**A TGC | –54 [–13] | –321 [+6] | –267 [+19] | –48 [–10] | –333 [–58] | –285 [–48] |
| **Z2** | 5′-GTG A**Z**A TGC | –46 [–5] | –336 [–9] | –290 [–4] | ND | ND | ND |

[a] See Table 4 for conditions.

**Table 6**

Pyrene absorption maxima for single stranded pyrene-functionalized 2′-amino-α-L-LNA and the corresponding duplexes with DNA/RNA complements.[a]

| | | $\lambda_{max}$ ($\Delta\lambda_{max}$)/ nm | | | | | | | | | | | |
|---|---|---|---|---|---|---|---|---|---|---|---|---|---|
| B = | | W | | | X | | | Y | | | Z | | |
| ON | Sequence | ss | + DNA | + RNA | ss | + DNA | + RNA | ss | + DNA | + RNA | ss | + DNA | + RNA |
| **B1** | 5′-G**B**G ATA TGC | 348 | 350 [+2] | 349 [+1] | 349 | 351 [+2] | 351 [+2] | 350 | 351 [+1] | 352 [+2] | 346 | 348 [+2] | 348 [+2] |
| **B2** | 5′-GTG A**B**A TGC | 347 | 351 [+4] | 349 [+2] | 348 | 353 [+5] | 351 [+3] | 346 | 351 [+5] | 351 [+5] | 346 | 347 [+1] | 346 [±0] |
| **B3** | 5′-GTG ATA **B**GC | 348 | 351 [+3] | 350 [+2] | 350 | 354 [+4] | 351 [+1] | 348 | 351 [+3] | 351 [+3] | ND | ND | ND |
| **B4** | 3′-CAC **B**AT ACG | 348 | 350 [+2] | 348 [±0] | 348 | 351 [+3] | 349 [+1] | 350 | 351 [+1] | 351 [+1] | 346 | 347 [+1] | 346 [±0] |
| **B5** | 3′-CAC TA**B** ACG | 348 | 350 [+2] | 349 [+1] | 348 | 351 [+3] | 351 [+3] | 346 | 351 [+5] | 352 [+6] | 346 | 348 [+2] | 347 [+1] |

[a] Measurements were performed at room temperature on a spectrophotometer in the range 300-400 nm, using a quartz optical cell with a 1.0 cm path length and same conditions as for thermal denaturation experiments.